Applied Physics Letters ARTICLE scitation.org/journal/apl

Pressure effects on the lattice vibrations and ultrafast photocarrier dynamics in 2*H*–TaS_2

Cite as: Appl. Phys. Lett. **117**, 101105 (2020); doi: 10.1063/5.0018615
Submitted: 16 June 2020 · Accepted: 31 August 2020 ·
Published Online: 11 September 2020

Kai Zhang,[1] Huachao Jiang,[1] Jin Yang,[1] Jie Zhang,[1] Zhi Zeng,[1] Xiaojia Chen,[1,2] and Fuhai Su[1,a)]

AFFILIATIONS

[1]Key Laboratory of Materials Physics, Institute of Solid State Physics, HFIPS, Chinese Academy of Sciences, Hefei 230031, China
[2]Center for High Pressure Science and Technology Advanced Research, Shanghai 201203, China

[a)]Author to whom correspondence should be addressed: fhsu@issp.ac.cn

ABSTRACT

Vibrational properties and ultrafast photocarrier dynamics of 2*H*–TaS_2 under pressures are studied by the experiments of Raman scattering and femtosecond time resolved spectroscopy. With increasing pressure, the linewidth of two-phonon Raman mode broadens, especially features with a sudden rapid increase above 10 GPa. Meanwhile, the ultrafast dynamics show that the fast decay through optical phonon scattering is significantly suppressed in amplitude and prolonged in lifetime; however, the weight of the slow decay component originating from acoustic phonon scattering is enhanced at high pressures. Furthermore, the electron-phonon (e-ph) coupling constant, λ_q, and the density of states (DOS) near the Fermi level, N(0), are evaluated qualitatively, which reveals a drastic decrease in e-ph coupling strength and a sudden increase in the DOS beyond 10 GPa. This turning pressure is consistent with the critical point where T_c of superconductivity peaks while the charge density wave (CDW) vanishes, indicating the direct correlations between λ_q, N(0), superconductivity, and the CDW under pressure. The anomaly of the DOS may imply the occurrence of a topological transition of the electronic structure. Our work not only provides valuable information for the understanding of competition between the CDW and superconductivity in 2*H*–TaS_2 but also may open up a routine to unveil the pressure-induced electronic topological transition.

Transition metal dichalcogenides (TMDs), as the layered structure bonded with van der Waals force, exhibit tremendous novel properties, such as charge density wave (CDW), superconductivity, extremely large magnetoresistance, and topological transition. The TMDs always serve as good candidates to study the origin of the CDW orders benefiting from not only the relatively simple structure but also the high energies of the CDW orders. These materials also have drawn much attention since the discovery of the delicate competitive behaviors between CDW orders and superconductivity.[1–3] Since the CDW also emerges in some cuprates,[4,5] the exploration of the origin of the CDW orders becomes increasingly important to dredge up the mystery about the superconductivity (SC) mechanism. Among TMDs, 2*H*–TaS_2 is a typical correlated electron material, which hosts both an incommensurate CDW and a superconducting transition at 78 K and 0.8 K, respectively.[6,7] The occurrences of the CDW and superconducting transitions result in significant anomalies on the electrical and thermal transport properties.[7–10] In the Raman scattering measurement, the two-phonon mode was found to compete with the CDW amplitude mode, and the other vibrational modes also showed anomalous behaviors at around the CDW lock-in temperature because of the CDW modulation.[8] Pressure is an efficient way to regulate the Fermi surface by compressing the lattice structure. For 2*H*–TaS_2, the electrical transport measurements as well as the Raman scattering studies reveal that the lock-in temperature of the CDW reduces with increasing pressure, whereas the superconducting transition temperature behaves in the opposite way,[11–14] which is consistent with the competitive scenario between CDW and SC orders. The low temperature angle resolved photoemission spectroscopy measurement evidences that the CDW distortion in 2*H*–TaS_2, like in other 2*H*-polytypes of TMDs, originates from the strong *q*-dependent electron-phonon (e-ph) coupling.[15] This strong e-ph interaction is the major force to drive the anomalous behaviors on the electrical transport, vibration, thermodynamics, etc.[15,16] Therefore, it is essential to access the evolution of e-ph coupling with pressure in order to deeply understand the underlying physics for the CDW and SC.

Femtosecond time-resolved spectroscopy (fs-TRS) is a powerful tool to detect the interaction mechanism among different excitations, such as hot electrons, phonons, and excitons, by distinguishing their different lifetimes and amplitudes at which the system translated from the nonequilibrium state to the equilibrium state. In general, the

two-temperature model (TTM) developed earlier[17–20] can be used to extract e-ph coupling information from the femtosecond pump-probe measurements. However, in this model, the electron–electron (e–e) collisions and the e-ph relaxation process are considered separately due to the assumption that the e–e collision time is much shorter than the e-ph relaxation time and, thus, has some limitations, such as in the strongly correlated electron systems. Furthermore, Groeneveld *et al.*,[21] Gusev and Wright,[22] and Kabanov and Alexandrov.[23] established an analytical nonequilibrium model (NEM) connecting the e-ph relaxation time with the e-ph interaction by considering the condition that electrons and phonons are out of equilibrium simultaneously. Based on the models, fs-TRS has been successfully applied to obtain the e-ph coupling parameter in superconductors and semimetals.[24,25]

Here, we combine the Raman scattering spectroscopy and fs-TRS techniques to investigate the vibrational properties and ultrafast dynamics in 2*H*–TaS_2 under pressure. We find that the linewidth of the two-phonon mode shows an anomalous change at around 10 GPa, corresponding to the critical pressure where the CDW order vanishes. Meanwhile, the pressure behavior of ultrafast photocarrier dynamics also manifests anomaly, featured with a sudden increase in the relaxation time constant, under the same pressure. The strength of the electron-phonon coupling under pressure is analyzed. Our work provides a groundwork to the understanding of the charge density wave orders in transition metal dichalcogenides.

In this experiment, the high-quality single crystal 2*H*–TaS_2 was bought from 2D materials company.[8] The high-pressure condition for both Raman and fs-TRS measurements was obtained using a diamond anvil cell (DAC) with the anvil culet of 300 μm. The transmission medium was argon, and the ruby fluorescence method was applied to determine the pressure. The sample loaded in the DAC was exfoliated mechanically in order to guarantee the fresh and smooth surface. The Raman scattering spectra were obtained by using a 488 nm sapphire laser line. The excited laser power was about 2 mW, and the beam was focused on the samples by a ×20 objective. The back-scattering light was collected by a CCD detector equipped with a 1800 g/mm grating (designed by Princeton instruments).

The block scheme of the fs-TRS is depicted in Fig. 1. A Ti:sapphire femtosecond oscillator (Mira F900, Coherent) was employed to deliver the laser pulses with a pulse duration of 150 fs, a central wavelength of 800 nm, and a repetition rate of 76 MHz, which was divided into two portions for the pump and probe, respectively. The pump beam was modulated by an acoustic optical modulator with 1 MHz repetition. The probe pulse passes through a hollow retroreflector loaded on a motorized translation stage that controls the pump-probe time delay. The cross-polarized pump (*s*-polarization) and probe (*p*-polarization) beams were spatially separated by a polarized beam splitter (PBS) cube and, then, focused onto the sample inside the DAC with spot diameters of ∼9 and ∼4 μm by an objective lens, respectively. The reflected probe pulses pass through the PBS again, which further suppress scattered light from the orthogonally polarized pump. The reflected probe signal was detected by a biased silicon photodetector and a RF lock-in amplifier. The pump fluence on the sample is set in the range of 70–370 μJ/cm^2. The ratio between pump and probe fluences on the sample is about 5:1. Both Raman spectroscopy and fs-TRS were performed at room temperature.

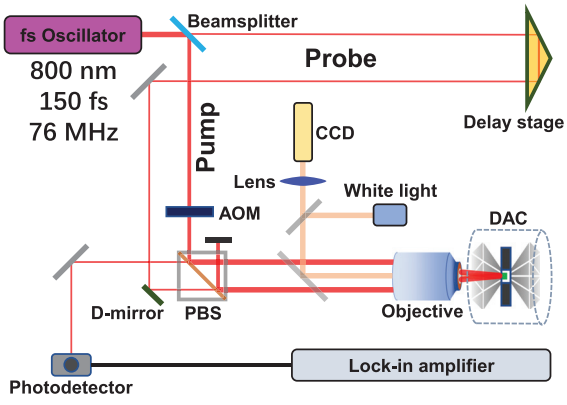

FIG. 1. Block scheme of the fs-TRS setup. AOM: acoustic optical modulator; PBS: polarized beam splitter.

Raman spectra of 2*H*–TaS_2 with the pressure ranging from 0 to 40 GPa are presented in Fig. 2(a). All the spectra have been subtracted a constant background. 2*H*–TaS_2 exhibits four peaks at ambient pressure, A_{1g}, E^1_{2g}, E^2_{2g} modes, and a typical two-phonon mode.[8,26] As can be seen, all of the Raman modes show blueshift with increasing pressure. The Raman shifts and full width at half maximum (FWHM) for A_{1g}, E^2_{2g} modes, and two-phonon mode are extracted using Lorentz functions fitting and are shown in Figs. 2(b)–2(d) as a function of pressure. The E^1_{2g} mode is too weak and cannot be fitted well. The frequency of the rigid-layer E^2_{2g} mode exhibits a nonlinear asymptotic increasing trend with increasing pressure. Similar pressure behavior can also be found in the FWHM of this mode. This may indicate that the layered structure of 2*H*–TaS_2 gradually merges into three-dimensional bulk at high pressure. The frequency of the A_{1g} mode also increases with increasing pressure. However, the FWHM of the A_{1g} mode is almost independent of external pressure, which can be attributed to the multiple scattering mechanism including the enhancement of the anharmonic scattering process, increase in the Raman scattering cross section, etc. As shown in Fig. 2(d), the frequency of the two-phonon mode increases as the pressure is increased.

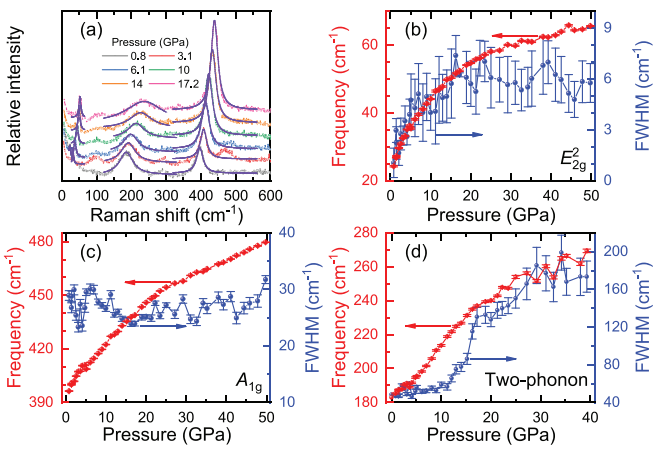

FIG. 2. (a) Raman spectra of 2*H*–TaS_2 at high pressures. The spectra have been displaced vertically for clarification. The fitted lines of the E^2_{2g}, A_{1g}, and two-phonon modes by Lorentz functions are also presented (solid lines). (b)–(d) Pressure dependence of the frequency and FWHM of these modes.

It is interesting that the FWHM of the two-phonon mode presents an initial gently increase up to 10 GPa, followed by rapid augment at higher pressure. Since no any Raman mode shows discontinuousness in the frequency around 10 GPa, such an abnormal pressure behavior in the FWMH of the two-phonon mode cannot be attributed to the lattice abruption. Earlier studies evidenced that the two-phonon mode shows a competition relation with the CDW modes. This mode origins from a soft-phonon branch and has a correlation with e-ph coupling and the DOS at the Fermi level.[8,27] Therefore, the anomaly of pressure dependence of the FWMH implies the dramatical changes in e-ph interactions and the DOS, which will be discussed later.

Now, we turn to the discussions on the photocarrier dynamics of 2*H*–TaS_2 under pressure. Figure 3(a) presents the transient differential reflectivity (DR), ΔR/R, acquired by fs-TRS at different pressures. As shown in Fig. 3(a), the relaxation dynamics indicated by the DR signal contains an initial fast decay component and subsequent long-live slow decay in the studied pressure range. With increasing pressure, the amplitude of the DR signal is decreased and the relaxation process is prolonged. Since the 2*H*–TaS_2 is a band metal without direct interband recombination, the fast decay should be attributed to the energy relaxation of the photocarrier through optical phonon scattering. We find that the slow decay component can last at least 500 ps and the DR signal does not go back to zero in our measurement time range. Such a long relaxation dynamics corresponds to the energy dissipation through the acoustic phonon interaction. For each pressure, the DR curve can be well fitted in terms of the biexponential function with an offset. In our study, we pay special attention to the fast decay in order to retrieve the e-ph coupling constant. From the best fittings, the obtained time constant τ_{fast} for the fast decay as a function of pressure is shown in Fig. 3(b). One can see that the τ_{fast} increases moderately with increasing pressure below 10 GPa, whereas it starts to rise drastically upon further compression, indicating pressure-induced weakening of the e-ph interaction. Another main feature as shown in Fig. 3(a) is that the fast component loses its intensity more pronouncedly than the slow component with pressure, which is in favor of the robustness of slow decay. We obtain the quantitative comparison between the fast and slow decay components by calculating the ratio between the amplitude of DR at 15 ps and peak signal (0 ps), defined as A_{15}/A_0. The pressure dependent A_{15}/A_0 is displayed in Fig. 3(c). It is noteworthy that the A_{15}/A_0 manifests an increasing effect with pressure similar to τ_{fast}, where the weight of the slow relaxation component from acoustic phonon scattering enhances remarkably above 10 GPa with respect to the optical phonon scattering. It should be mentioned that the pressure dependence for both A_{15}/A_0 and τ_{fast} shows somewhat abruptions around 5 GPa as marked in Figs. 3(b) and 3(c). Such anomalies are analogous to the pressure behavior of resistivity of 2*H*–TaS_2 at room temperature observed in earlier work, which was tentatively attributed to the shear-induced 2*H*-1*T* transition.[28] In the future, further *in situ* high-pressure experiments including second harmonic generation (SHG) and fs-TRS at low temperature may help to unravel the 2*H*-1*T* phase transition, as well as the impact on the CDW and SC.

In addition, we also measured the DR at different pump fluences for 2*H*–TaS_2 at the pressures of 4 and 12 GPa, respectively. As illuminated in Fig. 4(a), the amplitude of the DR signal increases with elevating pump power. The maximum DR amplitude scales up linearly with pump power as shown in the inset, which implies the absence of nonlinear absorption. In contrast, the relaxation time [see Fig. 4(c)] and A_{15}/A_0 [see Fig. 4(b)] of the DR signal are independent of pump power in our measured pump level at pressures. For 2*H*–TaS_2, the hot carriers with excess energy above the Fermi level can be injected immediately using the femtosecond laser pulse, which is followed by a rapid thermalization through e–e scattering and e-ph scattering and formation of quasi Fermi-Dirac (QFD) distributions. In general, the excess energy of the out-of-equilibrium hot photocarriers is primarily dissipated through high-frequency optical phonon scattering until a level lower than the corresponding optical phonon frequency; subsequently, the e-ph scatterings via low-frequency acoustic phonons dominate because the optical phonon emission is inefficient for

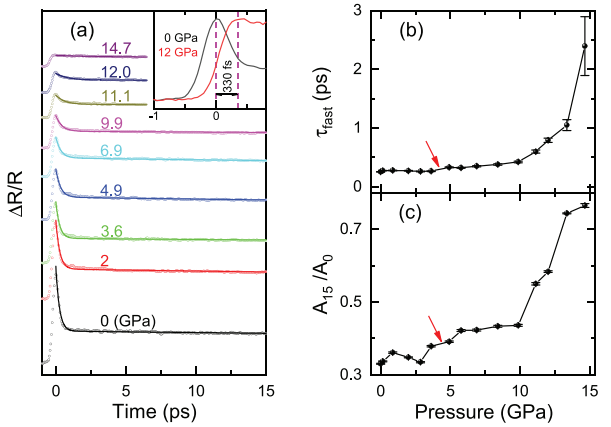

FIG. 3. (a) Transient differential reflectivity ΔR/R of 2*H*–TaS_2 at different pressures. The fitted lines by a biexponential function are also presented (solid lines). The inset is the zoom-in raw spectra at 0 and 12 GPa. (b) and (c) Pressure dependence of the fitted fast decay time τ_{fast} and the intensity ratio A_{15}/A_0 between the DR values at 15 ps and peak position (0 ps). Anomalies at around 5 GPa are visible and noted by arrows.

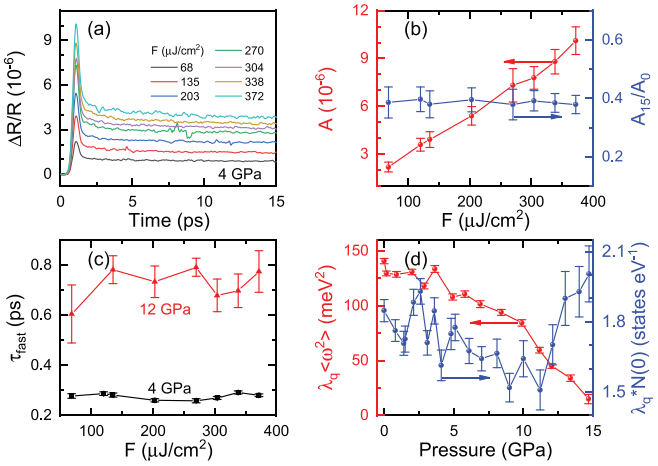

FIG. 4. (a) Photoinduced reflectivity change ΔR/R at 4 GPa for different pump fluences. (b) Fluence dependence of the summit amplitude and the amplitude ratio A_{15}/A_0. (c) Fluence dependence of the fast decay times τ_{fast} at 4 and 12 GPa. (d) Pressure dependence of the calculated second moment of the Eliashberg function $\lambda_q\langle\omega^2\rangle$ and $\lambda_q N(0)$.

low-energy carriers.[29] We suggest that the observed pressure evolution of photocarrier dynamics has a close correspondence to the changes of e-ph coupling and the DOS at the Fermi level. The large DOS near the Fermi level allows for the distribution of electrons in the low energy side as much as possible and, therefore, tends to reduce the carrier temperature of QFD. Under pressure, the electron-optical phonon coupling strength is reduced and the τ_{fast} is increased in 2*H*–TaS_2. Meanwhile, the DOS at the Fermi level is also increased as evidenced later, and the temperature of photoexcited hot carriers is decreased. As a result, the acoustic phonon scattering becomes robust compared with the optical phonon with increasing pressure, giving rise to the increase in relative intensity between slow and fast decay components as shown in Fig. 3(c). It should be mentioned that other factors such as the phonon bottleneck effect also likely slow down the photocarrier relaxation processes by the temporal accumulation of optical phonons.[30] Recently, Wu *et al.*[31] found the pressure-induced phonon bottleneck effect in Sr_2IrO_4. However, such an effect normally takes place for the high carrier injection level and depends on the pump fluence. This is not in line with our measured pump power dependence of photocarrier dynamics. Therefore, the contribution from the phonon bottleneck is negligible in our case.

Next, we quantitatively examine the pressure evolutions of the e-ph coupling and DOS. Since τ_{fast} is not sensitive to the pump fluence and the amplitude of the DR signal shows the linear relation, the contributions from e-e scattering cannot be distinguished. Therefore, the NEM is more suitable than the TTM in our case in order to extract the e-ph coupling information from the measured DR signal. In this model, the second moment $\lambda_q\langle\omega^2\rangle$ of the Eliashberg function can be obtained by[23,24] $\lambda_q\langle\omega^2\rangle = \frac{2\pi}{3}\frac{k_B T_l}{\hbar\tau_{e-ph}}$. Here, λ_q and $\langle\omega^2\rangle$ denote the e-ph coupling constant and mean square phonon frequency, respectively. T_l is the lattice temperature, and τ_{e-ph} is the relaxation time due to the electron-phonon interaction. Here, we replace τ_{e-ph} with the time constant of optical phonon scattering, τ_{fast}, and assume that the lattice temperature is close to room temperature. The obtained $\lambda_q\langle\omega^2\rangle$ under the ambient condition is $140 \pm 3\ \mathrm{meV}^2$. If only considering the term of $\langle\omega^2\rangle$ contributed by the two-phonon mode, λ_q is estimated to be about 0.27, which is slightly lower than the earlier theoretical calculation (~0.45).[32] This discrepancy may result from the underestimation of the lattice temperature T_l. The calculated $\lambda_q\langle\omega^2\rangle$ as a function of pressure is presented in Fig. 4(d). In view of the pressure-induced increase in phonon frequency as shown in Fig. 2, λ_q must be reduced with increasing pressure. On the other hand, as for the 2*H*-type TMDs system with strong e-ph interactions such as 2*H*–$NbSe_2$, 2*H*–TaS_2, and 2*H*–$TaSe_2$,[15,16] the e-ph coupling constant λ_q is also connected with the phonon vibration by the equation[33–35] $\lambda_q = \frac{1}{2\pi N(0)}\frac{\gamma_q}{\omega_q^2}$. Here, N(0) is the electronic density of states at the Fermi energy and γ_q and ω_q are the FWHM and frequency of the phonon mode, respectively, which corresponds to the two-phonon mode governed by the e-ph interaction in our case. The extracted λ_qN(0) values are presented in Fig. 4(d). It decreases slightly with increasing pressure first and then shows a remarkable increase as the pressure is beyond 10 GPa. Since the λ_q exhibits a decreasing trend with pressure, the sudden increase in λ_qN(0) implies the abnormal augment of N(0) above 10 GPa. We notice that the turning point accords with the pressure range where the CDW orders vanish and the T_c of the SC state concurrently peaks.[12] Therefore, our experimental results provide a roughly framework to explain such a competition between SC and CDW orders: (i) the weakening of the e-ph interaction should be responsible for the suppression of CDW order under pressure.[12] However, the decreasing trend of λ_q with pressure violates the modified McMillan formula, where the increased T_c with pressure should accompany with the increase in λ_q.[36] Recent works reported an enhancement in the T_c as the thickness of 2*H*–TaS_2 was reduced to the two-dimensional limit.[37,38] However, different theoretical interpretations have been proposed in terms of either the increase in effective electron-phonon coupling related to repulsive Coulomb interaction[37] or the increase in the DOS at the Fermi level induced by the suppression of CDW amplitude.[38] We suggest that the significant increase in N(0) can counteract the influence of e-ph coupling and contribute to the robustness of the SC state at about 10 GPa.[12] (ii) On the other hand, the distinct decrease in λ_q is able to restraint the SC order and reduce the T_c under higher pressure. Nevertheless, more experimental and theoretical works are required to fully understand the correlations between λ_q, N(0), SC, and CDW orders. In addition, it is somewhat surprising that our observed turning pressure for the linewidth and photocarrier dynamics at room temperature agree with the critical point of competition between SC and CDW orders,[12] which is expected to be accessible only at low temperature. We speculate that the Lifshitz transition,[39] i.e., Fermi surface topological transition, in 2*H*–TaS_2 takes place around 10 GPa, which likely gives rise to substantial modifications of the DOS and e-ph coupling. Indeed, such a kind of phase shift of DR signals as shown in the inset of Fig. 3(a) can be taken as signatures for topological transition of the electronic structure.[40] In general, the Lifshitz transition is not accompanied by the lattice abruption and then hardly identified by Raman and resistance measurements. Different from steady diagnosis methods such as electric transport and optical absorption spectroscopy, fs-TRS permits the excitation and detection of out-of-equilibrium photocarriers away from band extrema, which is more sensitive to the energy dispersion than the corresponding steady-state carriers. Therefore, fs-TRS may provide an alternative routine to probe the topological changes of electronic states under pressure.

In summary, we have studied pressure tuning on the electron-phonon interaction and electronic structure in 2*H*–TaS_2 by combining measurements of Raman scattering spectroscopy and fs-TRS. The linewidth of the two-phonon mode shows an initial slight increase, however, followed by prominent broadening above 10 GPa. Fs-TRS reveals that the time constant originating from optical phonon scattering is dramatically prolonged; meanwhile, the energy relaxation through acoustic phonon scattering dominates for pressures above 10 GPa. The anomalies of pressure behavior in two-phonon vibration and photocarrier relaxation in 2*H*–TaS_2 emphasize a sudden weakening and increase in e-ph coupling and the DOS above this critical pressure, respectively. In particular, the anomaly of the DOS at high pressures may be a signature of Lifshitz transition, which needs deeper theory and experimental investigations. We believe that this work provides important complementary insights into the pressure effects of the electrical structure in 2*H*–TaS_2 and also helps to understand the interactions between the superconductivity state and CDW order.

This work was supported by the National Natural Science Foundation of China (Grant Nos. 11774354, 51672279, 51727806, and 11874361), Science Challenge Project (No. TZ2016001), CAS

Innovation Grant (No. CXJJ-19-B08), and CASHIPS Director's Fund (Grant No. YZJJ201705).

DATA AVAILABILITY

The data that support the findings of this study are available from the corresponding author upon reasonable request.

REFERENCES

[1]R. Sooryakumar and M. V. Klein, Phys. Rev. Lett. **45**, 660–662 (1980).
[2]M. A. Méasson, Y. Gallais, M. Cazayous, B. Clair, P. Rodiere, L. Cario, and A. Sacuto, Phys. Rev. B **89**, 060503 (2014).
[3]R. Grasset, T. Cea, Y. Gallais, M. Cazayous, A. Sacuto, L. Cario, L. Benfatto, and M. A. Méasson, Phys. Rev. B **97**, 094502 (2018).
[4]W. D. Wise, M. C. Boyer, K. Chatterjee, T. Kondo, T. Takeuchi, H. Ikuta, Y. Wang, and E. W. Hudson, Nat. Phys. **4**, 696–699 (2008).
[5]T. Wu, H. Mayaffre, S. Krämer, M. Horvatić, C. Berthier, W. N. Hardy, R. Liang, D. A. Bonn, and M. H. Julien, Nature **477**, 191–194 (2011).
[6]S. Nagata, T. Aochi, T. Abe, S. Ebisu, T. Hagino, Y. Seki, and K. Tsutsumi, J. Phys. Chem. Solids **53**, 1259–1263 (1992).
[7]J. P. Tidman, O. Singh, A. E. Curzon, and R. F. Frindt, Philos. Mag. **30**, 1191–1194 (1974).
[8]K. Zhang, Z. Y. Cao, and X. J. Chen, Appl. Phys. Lett. **114**, 141901 (2019).
[9]J. M. E. Harper, T. H. Geballe, and F. J. DiSalvo, Phys. Rev. B **15**, 2943–2951 (1977).
[10]S. J. Hillenius and R. V. Coleman, Phys. Rev. B **18**, 3790–3798 (1978).
[11]R. Delaplace, P. Molinie, and D. Jerome, J. Phys. Lett. **37**, 13 (1976).
[12]R. Grasset, Y. Gallais, A. Sacuto, M. Cazayous, S. Mañas-Valero, E. Coronado, and M. A. Méasson, Phys. Rev. Lett. **122**, 127001 (2019).
[13]D. C. Freitas, P. Rodiere, M. R. Osorio, E. Navarro-Moratalla, N. M. Nemes, V. G. Tissen, L. Cario, E. Coronado, M. García-Hernández, S. Vieira, M. Núñez-Regueiro, and H. Suderow, Phys. Rev. B **93**, 184512 (2016).
[14]X. M. Zhao, K. Zhang, Z. Y. Cao, Z. W. Zhao, V. V. Struzhkin, A. F. Goncharov, H. K. Wang, A. G. Gavriliuk, H. K. Mao, and X. J. Chen, Phys. Rev. B **101**, 134506 (2020).
[15]K. Wijayaratne, J. Zhao, C. Malliakas, D. Y. Chung, M. G. Kanatzidis, and U. Chatterjee, J. Mater. Chem. C **5**, 11310–11316 (2017).
[16]F. Weber, S. Rosenkranz, J. P. Castellan, R. Osborn, R. Hott, R. Heid, K. P. Bohnen, T. Egami, A. H. Said, and D. Reznik, Phys. Rev. Lett. **107**, 107403 (2011).
[17]M. I. Kaganov, E. M. Lifshitz, and L. V. Tanatarov, Sov. Phys. JETP **4**, 173 (1957).
[18]S. I. Anisimov, B. L. Kapeliovich, and T. L. Perelman, Zh. Eksp. Teor. Fiz. **66**, 375–377 (1974).
[19]P. B. Allen, Phys. Rev. Lett. **59**, 1460 (1987).
[20]S. D. Brorson, A. Kazeroonian, J. S. Moodera, D. W. Face, T. K. Cheng, E. P. Ippen, M. S. Dresselhaus, and G. Dresselhaus, Phys. Rev. Lett. **64**, 2172 (1990).
[21]R. H. M. Groeneveld, R. Sprik, and A. Lagendijk, Phys. Rev. B **51**, 11433 (1995).
[22]V. E. Gusev and O. B. Wright, Phys. Rev. B **57**, 2878 (1998).
[23]V. V. Kabanov and A. S. Alexandrov, Phys. Rev. B **78**, 174514 (2008).
[24]C. Gadermaier, A. S. Alexandrov, V. V. Kabanov, P. Kusar, T. Mertelj, X. Yao, C. Manzoni, D. Brida, G. Cerullo, and D. Mihailovic, Phys. Rev. Lett. **105**, 257001 (2010).
[25]C. Gadermaier, V. V. Kabanov, A. S. Alexandrov, L. Stojchevska, T. Mertelj, C. Manzoni, G. Cerullo, N. D. Zhigadlo, J. Karpinski, Y. Q. Cai, X. Yao, Y. Toda, M. Oda, S. Sugai, and D. Mihailovic, Phys. Rev. X **4**, 011056 (2014).
[26]S. Sugai, K. Murase, S. Uchida, and S. Tanaka, Solid State Commun. **40**, 399–401 (1981).
[27]M. V. Klein, Phys. Rev. B **24**, 4208 (1981).
[28]A. J. Grant, T. M. Griffiths, G. D. Pitt, and A. D. Yoffe, J. Phys. C **7**, L249 (1974).
[29]A. Othonos, J. Appl. Phys. **83**, 1789 (1998).
[30]W. Pötz, Phys. Rev. B **36**, 5016 (1987).
[31]Y. Wu, X. Yin, J. Hasaien, Y. Ding, and J. Zhao, Chin. Phys. Lett. **37**, 047801 (2020).
[32]G. Y. Guo and W. Y. Liang, J. Phys. C **20**, 4315 (1987).
[33]P. B. Allen and R. Silberglitt, Phys. Rev. B **9**, 4733 (1974).
[34]A. Shukla, M. Calandra, M. d'Astuto, M. Lazzeri, F. Mauri, C. Bellin, M. Krisch, J. Karpinski, S. M. Kazakov, J. Jun, D. Daghero, and K. Parlinski, Phys. Rev. Lett. **90**, 095506 (2003).
[35]X. J. Chen, V. V. Struzhkin, Z. Wu, R. E. Cohen, S. Kung, H. K. Mao, and R. J. Hemley, Phys. Rev. B **72**, 094514 (2005).
[36]W. L. McMillan, Phys. Rev. **167**, 331 (1968).
[37]E. Navarro-Moratalla, J. O. Island, S. Manas-Valero, E. Pinilla-Cienfuegos, A. Castellanos-Gomez, J. Quereda, G. Rubio-Bollinger, L. Chirolli, J. A. Silva-Guillén, N. Agraït, G. A. Steele, F. Guinea, H. S. J. van der Zant, and E. Coronado, Nat. Commun. **7**, 11043 (2016).
[38]Y. Yang, S. Fang, V. Fatemi, J. Ruhman, E. Navarro-Moratalla, K. Watanabe, T. Taniguchi, E. Kaxiras, and P. Jarillo-Herrero, Phys. Rev. B **98**, 035203 (2018).
[39]I. M. Lifshitz, Sov. Phys. JETP **11**, 1130 (1960).
[40]C. Giannelti, G. Coslovich, F. Cilento, G. Ferrini, H. Eisaki, N. Kaneko, M. Greven, and F. Parmigiani, Phys. Rev. B **79**, 224502 (2009).